

1 **ABSTRACT**

2 This paper reports a new class of thin film nanocomposite (TFN) membranes
3 incorporated with covalent organic frameworks (COFs) nanoparticles in the polyamide
4 skin layer and having enhanced solvent (ethanol) permeation flux and high solute
5 rejection for organic solvent nanofiltration (OSN). These OSN membranes were
6 prepared via interfacial polymerization of m-phenylenediamine (MPD) and trimesoyl
7 chloride with the presence of COFs nanoparticles in the MPD aqueous solution,
8 followed by chemical crosslinking and solvent activation. The prepared TFN
9 membranes exhibited an improved surface hydrophilicity and a decreased skin layer
10 thickness, which leading to a 46.7% increment in the ethanol permeance (up to 79.8 L
11 m⁻² h⁻¹ MPa⁻¹) compared to those COFs-free membranes, as well as an increased
12 Rhodamine B (479 Dalton) rejection (up to 99.4%). Moreover, our prepared TFN OSN
13 membranes exhibited an excellent solvent resistance after being statically immersed in
14 *N, N*-dimethylformamide (DMF) at ambient temperature over 100 days, and after being
15 consecutively cross-flow filtrated using Rose Bengal/DMF solution at ambient
16 temperature over 7 days, both with no significant changes in the separation performance.
17 Furthermore, they showed only minor decrease in flux and rejection after being
18 statically immersed in DMF at 80 °C over 14 days, which provides a strong potential in
19 OSN applications.

20

21 **Keywords:** Covalent organic frameworks (COFs); Organic solvent nanofiltration
22 (OSN); Thin film nanocomposite (TFN); Interfacial polymerization (IP)

1 **1. Introduction**

2 Organic solvent nanofiltration (OSN), also known as solvent resistant
3 nanofiltration (SRNF), is an emerging technology for molecular separation and
4 purification of organic substances [1-4]. The core component of OSN technology is
5 OSN membranes, which should provide not only high solvent permeance and high
6 solute rejection, but good solvent resistance as well.

7 Most OSN membranes (reported in literatures or used commercially) belong to the
8 family of integrally skinned asymmetric (ISA) membranes prepared by phase inversion
9 [2]. Generally speaking, most ISA membranes suffered from inherent limitations of
10 tight skin layer, which resulted in a relative low solvent permeance [5]. However, there
11 are some efforts to promote the permeance of ISA membranes through using novel
12 materials such as PIM, metal organic frameworks (MOFs), or graphene oxide [6-8].
13 Recently, thin film composite (TFC) membranes which are characterized by an ultra-
14 thin “separation barrier layer” prepared via interfacial polymerization (IP) on the top
15 surface of a chemically different porous substrate have gained much attention for OSN
16 applications [9]. Livingston et al. [10] prepared high flux TFC membranes via IP
17 reaction of m-phenylenediamine (MPD) and trimesoyl chloride (TMC) on crosslinked
18 polyimide (PI) substrates followed by a solvent activation process, and increased the
19 methanol flux from 5.0 up to 15.3 L m⁻² h⁻¹ MPa⁻¹ without sacrificing selectivity.
20 Peinemann et al. [11] fabricated a type of new OSN membranes by IP using catechin
21 as the monomer of the aqueous phase and terephthaloyl chloride as the monomer of the
22 organic phase on a cellulose support. The fabricated membrane showed a DMF

1 permeance of $14.0 \text{ L m}^{-2} \text{ h}^{-1} \text{ MPa}^{-1}$ with a rejection of 92% for Amido-Black (617
2 Dalton).

3 The separation performance of polymeric membranes is always limited by the
4 trade-off effect between the solvent permeability and the solute selectivity [12]. Most
5 of the OSN membranes possess high solute selectivity but relative low solvent
6 permeability (or permeation flux). Recently, several approaches have been reported to
7 enhance the solvent flux of TFC-type membranes while maintaining high solute
8 rejection, including the adoption of aqueous additive [13], solvent activation [10], and
9 nanoparticles incorporation [14-16].

10 Nanoparticles incorporation has proved to be a promising approach to fabricate
11 thin film nanocomposite (TFN) membranes with improved separation performance. In
12 literatures, several types of additive nanoparticle materials, including MOFs [17],
13 graphene oxide [18], carbon nanotubes [19], MXene [20], zeolite [21], and silica
14 particles [22], have been investigated for the preparation of TFN membranes. For
15 instance, Guo et al. [23] incorporated a kind of MOF nanoparticles (surface-modified
16 UiO-66-NH₂) into the thin polyamide (PA) layer of the composite membranes and
17 significantly enhanced the pure methanol permeance from 103 up to $200 \text{ L m}^{-2} \text{ h}^{-1}$
18 MPa^{-1} , while maintained a rejection as high as 99% for tetracycline (444.4 Dalton).
19 Sorribas et al. [17] introduced another kind of MOF (MIL-101(Cr)) nanoparticles into
20 the PA active layer through IP reaction and increased the methanol permeance of the
21 prepared TFN membrane from 15 to $39 \text{ L m}^{-2} \text{ h}^{-1} \text{ MPa}^{-1}$ for methanol/polystyrene
22 solution, while maintaining the rejection as high as 98% for polystyrene (400 Dalton).

1 Yuan et al. [24] incorporated carbon dots into polyethyleneimine aqueous monomer
2 solution and used TMC hexane as the organic monomer solution to prepare TFN
3 membranes through IP and achieved a 54.3% increase of the pure isopropanol
4 permeance, which was up to $42.6 \text{ L m}^{-2} \text{ h}^{-1} \text{ MPa}^{-1}$.

5 Recently, covalent organic frameworks (COFs) as a new class of nanoparticles
6 have drawn intensive attention due to their specific characteristics such as porous
7 structures, relatively low density and desirable solvent stability by assembling organic
8 building blocks solely via strong covalent bonds [25-28]. COFs have been studied as
9 “filler” materials for the preparation of hybrid matrix membranes for desalination [29-
10 32], pervaporation (ethanol dehydration) [33], and gas separation [34]. COFs have not
11 only high organic solvent stability and thermal stability, but suitable pore size inside
12 their frameworks which may provide passageways for solvent molecules to penetrate
13 through without destroying the COFs structure. Moreover, the entire organic-organic
14 covalent bonds inside COFs endow them better affinity with organic polymers [35].
15 Therefore, COFs can be a good candidate as nanoparticle fillers for the preparation of
16 high performance and stable TFN membranes for OSN applications. However, till now,
17 no research work was reported to use COFs as an additive in the IP process to fabricate
18 TFN OSN membranes with complete covalent bonds.

19 In this work, we prepare a class of novel TFN OSN membranes with high
20 separation and solvent resistance performance via incorporating COFs nanoparticles
21 with rich secondary amine (-NH-) groups into polyamide active layer. We
22 comprehensively investigated the effect of the monomers concentrations, the content of

1 COFs nanoparticles incorporated and the solvent activation time on the separation
2 performance of the prepared OSN membranes. Furthermore, we evaluated the solvent
3 resistance performance of the optimized COFs-incorporated OSN membranes by long-
4 term static immersion and consecutively cross-flow filtration with *N, N*-
5 dimethylformamide (DMF). The results presented in this study provide new insights
6 into the development of the high performance COFs-incorporated TFN membranes for
7 industrial OSN applications.

8

9 **2. Experimental**

10 **2.1. Material**

11 Polyimide (PI, Lenzing P84, in granule form) was purchased from Inspec Fibers
12 GmbH, Lenzing (Austria). Polyester (PE) non-woven fabric was purchased from Japan
13 Teijin Co., Ltd. M-phenylenediamine (MPD, 99.5%) was obtained from J&K Scientific
14 Ltd. Trimesoyl chloride (TMC, 98.0%) was purchased from Macklin Biochemical Co.,
15 Ltd. Melamine (99.5%), terephthalaldehyde (98.0%), polyethylene glycol (PEG) 400
16 (liquid form), 1,6-hexanediamine (HDA, 99%), acetone (99.5%), methanol (99.9%),
17 tetrahydrofuran (THF, 99.0%), dimethylsulfoxide (DMSO, 99.0%), Rhodamine B
18 (RDB, 479 Da) and Rose Bengal (RB, 1017 Da) were purchased from Sinopharm
19 Chemical Reagent Co., Ltd. Ethanol (99.7%), isopropyl alcohol (IPA, 99.7%), *n*-
20 hexane (98%), and *N, N*-dimethylformamide (DMF, 99.5%) were supplied by Tianjin
21 Fuyu Fine Chemical Co., Ltd. All the solvents and chemicals were chemical purity

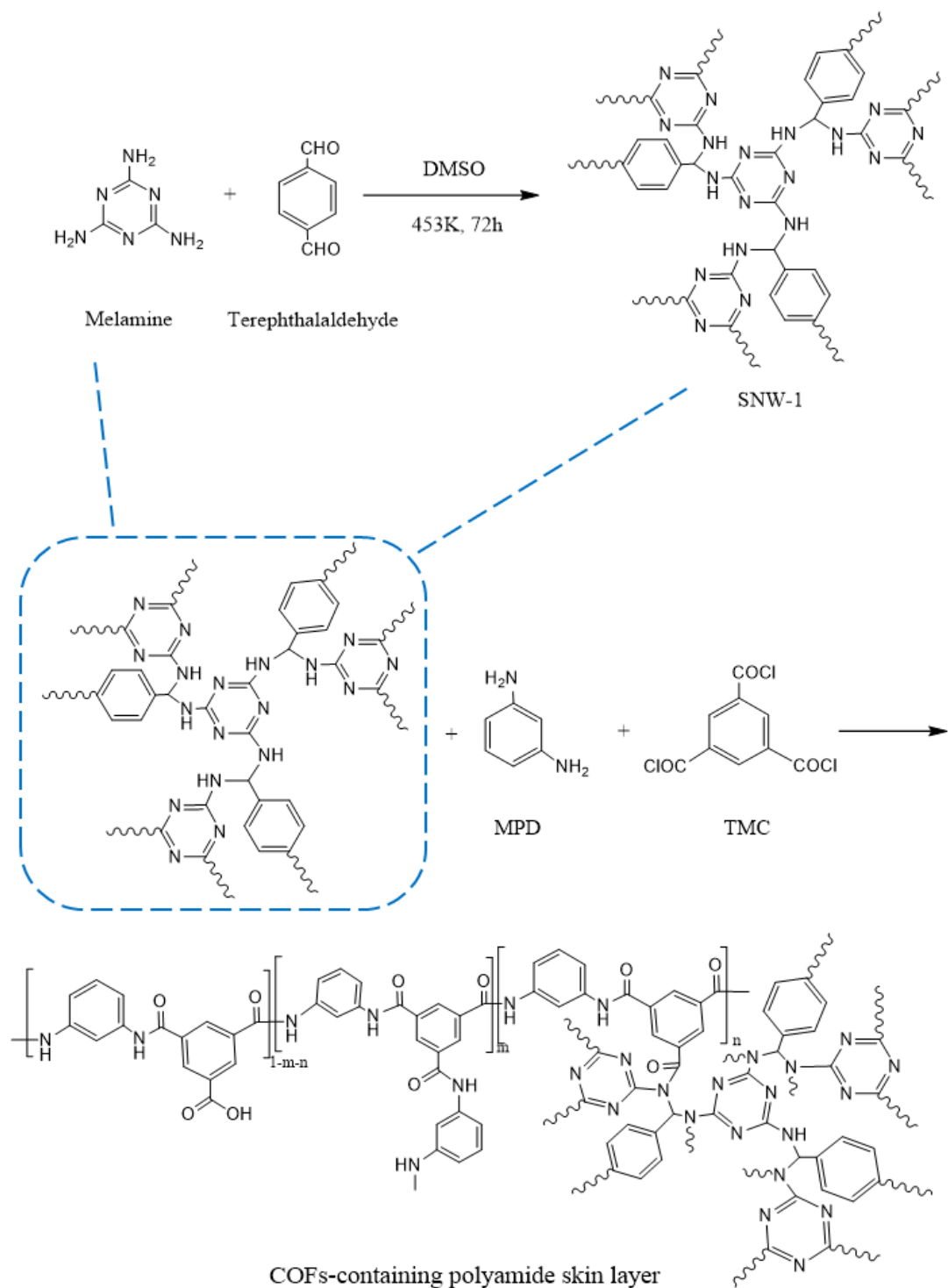
1 grade and were used without further purification. Deionized (DI) water was produced
2 by a Flom water purification system (Qingdao, China).

3 **2.2. Synthesis of COFs nanoparticles**

4 The COFs nanoparticles were synthesized following a literature procedure [36].
5 Briefly, 1.0 g melamine, 1.6 g terephthalaldehyde and 50 ml DMSO were put into a
6 round flask with a magnetic stirrer for mixing the solution mixture and a condenser for
7 refluxing the DMSO and water generated. The mixture was heated to 180 °C under
8 atmospheric pressure and was kept for 3 days under a nitrogen atmosphere. Gradually,
9 a kind of off-white colored solid of COFs nanoparticles was formed. Then, the mixture
10 was cooled to ambient temperature and was subsequently filtrated by a Büchner funnel
11 and the obtained COFs nanoparticles were sequentially washed with acetone, DMF and
12 THF. The COFs nanoparticles were further refined sequentially with THF and methanol
13 via Soxhlet extraction and each procedure was performed using 350 ml of the pure
14 solvent for 12 h. Afterwards, the COFs nanoparticles were dried under vacuum at 120
15 °C overnight. The obtained dry COFs powder was termed as SNW-1 [36].

16 Certain amount of the SNW-1 powder was dispersed into DI water by ultrasound
17 for 12 h and then was centrifuged at 4500 rpm for 15 min. The obtained supernatant
18 SNW-1 nanoparticles aqueous mixture was used for the preparation of TFN OSN
19 membranes and the content of SNW-1 was calibrated via weighting method before
20 usage. It is worth noting that the pore size in SNW-1 is around 5 Å [30], which allows
21 the penetration of ethanol molecules (maximum dimension of 3.7 Å according to Wave
22 Function Spartan program [37] or kinetic diameter of 4.4 Å according to Chung et al.

1 [38]). The synthesis route of SNW-1 is illustrated in **Fig. 1**.



2

3 **Fig. 1.** The synthesis route of the SNW-1 [36] and the schematic formula of the

4 interfacial polymerization of the TFN membrane with the covalent incorporation of

5 SNW-1 nanoparticles.

1 **2.3. Preparation of the PI substrate**

2 The PI substrate was prepared via the phase inversion method according to our
3 previous work [39] and the detailed preparation procedure can also be seen in the
4 Supporting Information.

5 **2.4. Formation of TFC and TFN membranes**

6 For the preparation of the TFC membrane skin layers, the prepared PI substrate
7 was taped onto a glass plate with the skin layer facing upwards. The aqueous diamine
8 solution was prepared by dissolving certain amount of MPD in DI water, and was
9 poured onto the surface of the substrate and allowed to soak for 8 s. Then the solution
10 on the top surface of the substrate was gently drained off and the excess droplets were
11 removed by a squeegee roller. The diamine saturated substrate surface was dried in the
12 air for about 1 min. Afterward, a certain amount of TMC in n-hexane solution was
13 slowly poured onto the amine-loaded substrate surface. After 6 s of IP reaction, the
14 TMC solution was poured off and the entire sample was dried in the oven at 80 °C for
15 5 min. The formed membrane in this stage was denoted as “(PA/PI)” membrane.

16 Afterwards, the (PA/PI) membrane was immersed in a crosslinking bath of 10 wt%
17 HDA IPA solution at 60 °C for 1 h to improve the solvent resistance. The crosslinked
18 membrane was then removed from the crosslinking bath and was rinsed with ethanol,
19 followed by immersing in ethanol for at least 3 h to remove any residual solvent. The
20 HDA crosslinked membrane was termed as “(PA/PI)_X” membrane for short. Finally,
21 the crosslinked (PA/PI)_X membrane was treated with DMF at 80 °C for 30 min (unless
22 otherwise specified) for solvent activation to improve its separation performance. The

1 solvent-activated TFC membrane (now suitable for OSN testing) was termed as
2 “(PA/PI)_{XA}” membrane.

3 For the preparation of the COFs-incorporated TFN membranes, aqueous monomer
4 solutions containing the same MPD concentration as that of the above-mentioned
5 “(PA/PI) membrane” and 25-120 mg L⁻¹ SNW-1 nanoparticles were used to prepare
6 the TFN-OSN membranes, and the resulted membranes in each stage were similar to
7 those of the TFC (PA/PI) membranes and were termed as (PA-COFs-*c*/PI), (PA-COFs-
8 *c*/PI)_X, and (PA-COFs-*c*/PI)_{XA}, respectively, where *c* represented the content (mg L⁻¹)
9 of the SNW-1 nanoparticles in the aqueous diamine solution used for the IP reaction.

10 The schematic chemistry of the IP reaction between MPD and TMC in the
11 presence of the SNW-1 nanoparticles to create TFN membranes was shown in **Fig. 1**.
12 The -NH- groups of the SNW-1 nanoparticles could react with the -COCl groups of
13 TMC and form strong covalent bonds in the matrix of the PA skin layer [30], thus
14 resulting in TFN OSN membranes with stable covalent bonds structure between the
15 SNW-1 nanoparticles and the PA backbones.

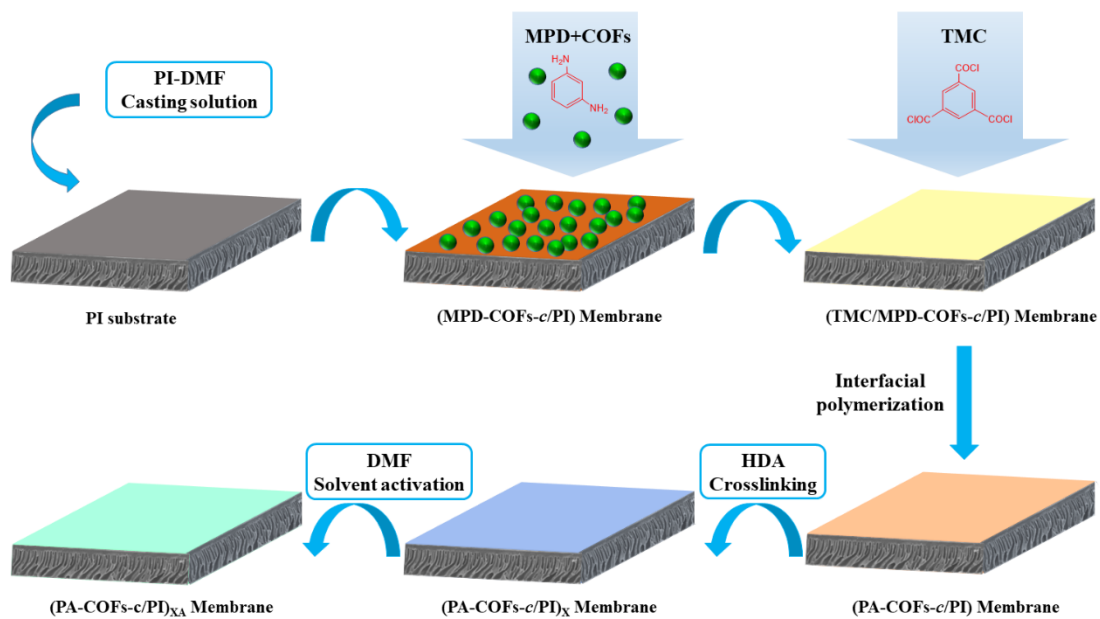
16 The brief description of each stage during the membrane preparation was
17 summarized in **Table 1**.

18 **Table 1** The brief description of each stages during the membrane preparation.

Membrane type	Stage	Detail description
	PI substrate	Phase inversion of PI casting solution
TFC	(PA/PI)	Interfacial polymerization between MPD and TMC

	$(PA/PI)_X$	Chemical crosslinked with HDA
	$(PA/PI)_{XA}$	Solvent activation with DMF
	$(PA-COFs-c/PI)$	Interfacial polymerization between MPD+COFs and TMC
TFN	$(PA-COFs-c/PI)_X$	Chemical crosslinked with HDA
	$(PA-COFs-c/PI)_{XA}$	Solvent activation with DMF

1 The whole fabrication route for the TFN membrane is depicted in Fig. 2.



2

3 **Fig. 2.** Schematic illustration for the fabrication of the TFN-OSN membrane with

4 COFs incorporated inside the PA skin layer.

5

6 2.5. Characterizations

7 The chemical groups of the SNW-1 nanoparticles and the prepared membranes

8 under different conditions were detected using an attenuated total reflectance Fourier

9 transform infrared spectrometer (ATR-FTIR, Thermo Nicolet Magna-560). The

10 morphologies of the membranes and the size of the SNW-1 nanoparticles were

1 examined using a transmission electron microscope (TEM, HT-7700, Hitachi, Japan).
2 The elements composition and chemical bonding of the membrane surface were
3 determined using an X-ray photoelectron spectroscopy (XPS, Thermo ESCALAB
4 250XI, US). The crystallinity of SNW-1 was evaluated using Powder X-ray diffraction
5 (PXRD, D8 ADVANCE diffractometer, Bruker, Germany). The surface and cross-
6 sectional morphologies of the membranes were imaged using a scanning electron
7 microscopy (SEM, S-4800SEM, Hitachi, Japan). The surface roughness of the prepared
8 membranes was characterized by an atomic force microscopy (AFM, Agilent 5400
9 equipped with a dimension AFM scan head) and was further analyzed by a PICOVIEW
10 analysis software. The static water contact angle of the membranes surface was
11 measured by the sessile drop method using an automatic contact angle goniometer
12 (DSA-100, KRÜSS, Germany) at room temperature. Each sample was measured at
13 least three random locations and then an average value was obtained.

14 Prior to all the above characterization, membrane samples were pre-dried in a high
15 vacuum drying oven (at -0.095 MPa, 50 °C) for 24 h.

16 **2.6. Separation performance of the prepared membranes**

17 The separation performance of the prepared membranes, as well as the long-term
18 continuous cross-flow filtration test, was evaluated in terms of the solvent permeance
19 and the solute rejection using a laboratory-made cross-flow filtration system [40]. The
20 effective area of each membrane sheet was 28.26 cm². The membrane sheets were
21 placed into four cross-flow membrane cells in series. The schematic diagram and the
22 picture of the membrane performance evaluation setup is shown in **Fig. S1**. The

1 filtration test was carried out using a 100.0 mg L⁻¹ dyes solution and the temperature
2 of the solution was controlled at 25±1 °C using a mini automatic thermostat (HH-6,
3 Shuangjie, China). The permeate sample was collected as a function of time and was
4 weighted by an electric balance to determine the solvent permeance (P , L m⁻² h⁻¹ MPa⁻¹)
5 according to Eq. (1):

$$P = \frac{\Delta V}{A \cdot \Delta t \cdot \Delta p} \quad (1)$$

6 where ΔV (L) is the volume of the permeate collected in the time period Δt (h) under a
7 trans-membrane pressure Δp (MPa), A (m²) is the effective membrane area.

8 The solute (dye) rejection was calculated from Eq. (2):

$$R = \left(1 - \frac{C_p}{C_f}\right) \times 100\% \quad (2)$$

9 where C_p and C_f denote the dye concentrations in the permeate and in the feed solution,
10 respectively. The dye concentration was measured by using an ultraviolet and visible
11 spectrophotometer (METASH UV-5100, China).

12 The membranes were conditioned at 1.0 MPa using the test solution for about half
13 an hour prior to the measurement until the permeance reached a steady value, and then
14 the permeance and the rejection were periodically measured for each membrane sheet.
15 The average permeance and the rejection values were calculated as the mean values of
16 at least two different membrane sheets tested, the standard deviations were also
17 evaluated.

18 **2.7. Theoretical analysis of the skin layer pore size distribution**

19 Log-normal probability density function was employed to describe the pore size
20 distribution (the average pore radius r^* and the pore diameter deviation σ^*) inside the

1 skin layer of the OSN membranes [7, 41-45]. The pore size distribution model and the
 2 related equations used in the theoretical analysis of the pore size distribution in the skin
 3 layer were recently summarized in our recent work [39]. The log-normal distribution is
 4 as follows:

$$f_R(r) = \frac{1}{r\sqrt{2\pi b}} \cdot \exp\left\{-\frac{\left[\log\left(\frac{r+b}{r^*+\frac{b}{2}}\right)\right]^2}{2b}\right\} \quad (3)$$

$$b = \log\left[1.0 + \left(\frac{\sigma^*}{r^*}\right)^2\right] \quad (4)$$

5 where $f_R(r)$ denotes the log-normal probability density of the pore size in the skin layer.

6

7 **3. Results and discussion**

8 **3.1. Characterization of SNW-1 nanoparticles**

9 The FTIR spectrum of the SNW-1 nanoparticles is shown in **Fig. S2** (a). The band
 10 at 3366 cm^{-1} corresponds to the stretching vibration of the N-H group and the peaks
 11 located at 1557 cm^{-1} and 1470 cm^{-1} are ascribed to the quadrant and semicircle
 12 stretching of the triazine ring, proving that SNW-1 nanoparticles with desired
 13 functional structures/groups were successfully synthesized [36]. **Fig. S2** (b) recorded
 14 the characteristic diffraction peaks of SNW-1. The medium intensity peak at $2\theta = 19^\circ$
 15 indicated the amorphous state of the SNW-1 nanoparticles. The obtained SNW-1
 16 nanoparticles had an average size of about 20 nm and showed a uniform dispersion, as
 17 can be seen in **Fig. S2** (c, d). It is expected that the synthesized SNW-1 nanoparticles
 18 could be uniformly dispersed within the polymer matrix of the prepared OSN skin layer.

3.2. Characterizations of membranes

Fig. 3 shows the ATR-FTIR spectra of the membranes at different fabrication steps. The PI substrate exhibited strong absorptions at 1365 cm^{-1} (C-N stretching) [46], 1722 cm^{-1} ($\text{C}=\text{O}$ stretching), and 1779 cm^{-1} ($\text{C}=\text{O}$ stretching), which are representative peaks of the imide groups [13].

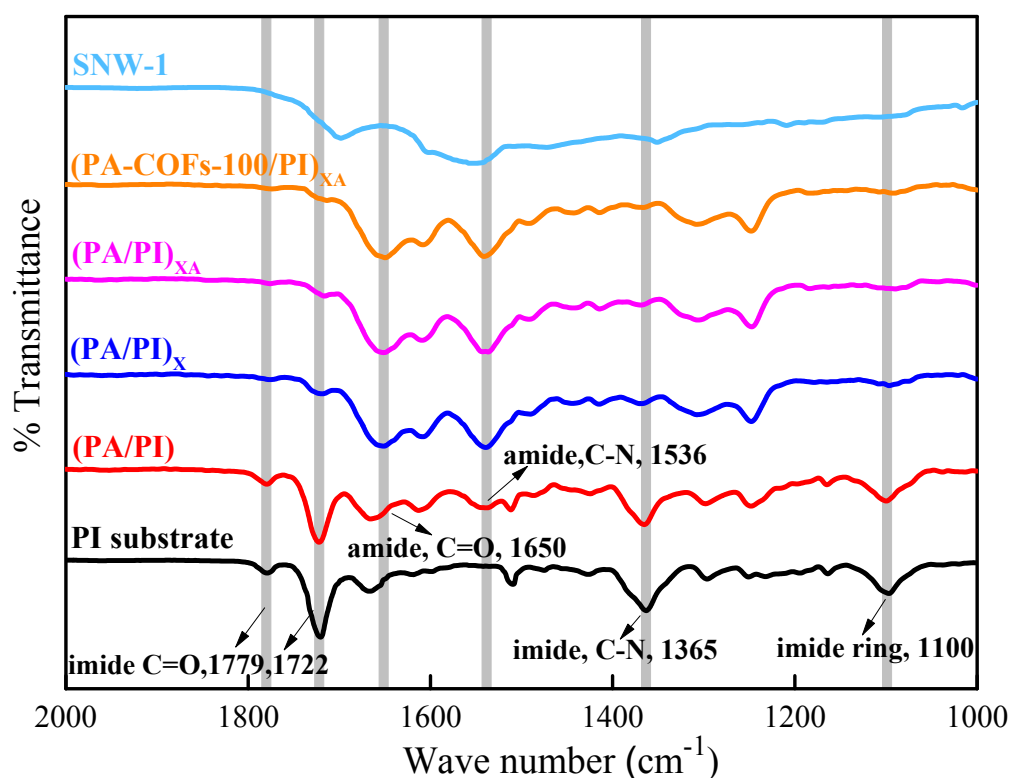


Fig. 3. ATR-FTIR spectra of the SNW-1, PI substrate, (PA/PI), (PA/PI)_x, (PA/PI)_{xA} and (PA-COFs-100/PI)_{xA} membranes.

The intensities of the above imide peaks reduced after the IP reaction, as can be seen from the spectrum of the (PA/PI) membrane in **Fig. 3**, while new peaks appeared at 1536 cm^{-1} (C-N stretching) and 1650 cm^{-1} ($\text{C}=\text{O}$ stretching) due to the formation of the amide groups [47] during the IP reaction, which confirmed the formation of the PA selective layer. It should be noted that the peaks of the (PA/PI) membrane came from

1 both layers (the PI substrate and the PA active layer) due to the relatively high
2 penetration depth (> 300 nm) of ATR-FTIR that far exceeded the PA layer thickness
3 [48]. So that the characteristic peaks of the imide groups belonging to the PI substrate
4 were still observed after the formation of the PA layer.

5 After the crosslinking with HDA, the characteristic peaks of the imide groups
6 almost vanished and the characteristic peaks of the amide groups increased obviously,
7 as can be seen on the spectrum of the $(\text{PA/PI})_X$ membrane. These changes indicated that
8 the PI substrate had been successfully crosslinked by HDA. The small imide peaks at
9 1365 cm^{-1} and 1722 cm^{-1} implied the existence of the unreacted imide groups inside
10 the crosslinked membrane [49].

11 After the solvent activation by DMF, the spectrum of the $(\text{PA/PI})_{XA}$ membrane
12 changed little compared with that of the $(\text{PA/PI})_X$ membrane. This clearly demonstrated
13 that the activation process did not influence the chemical structures of the crosslinked
14 OSN membrane, as the purpose of the solvent activation is only to dissolve some PA
15 oligomer fragments with low molecular weight [10].

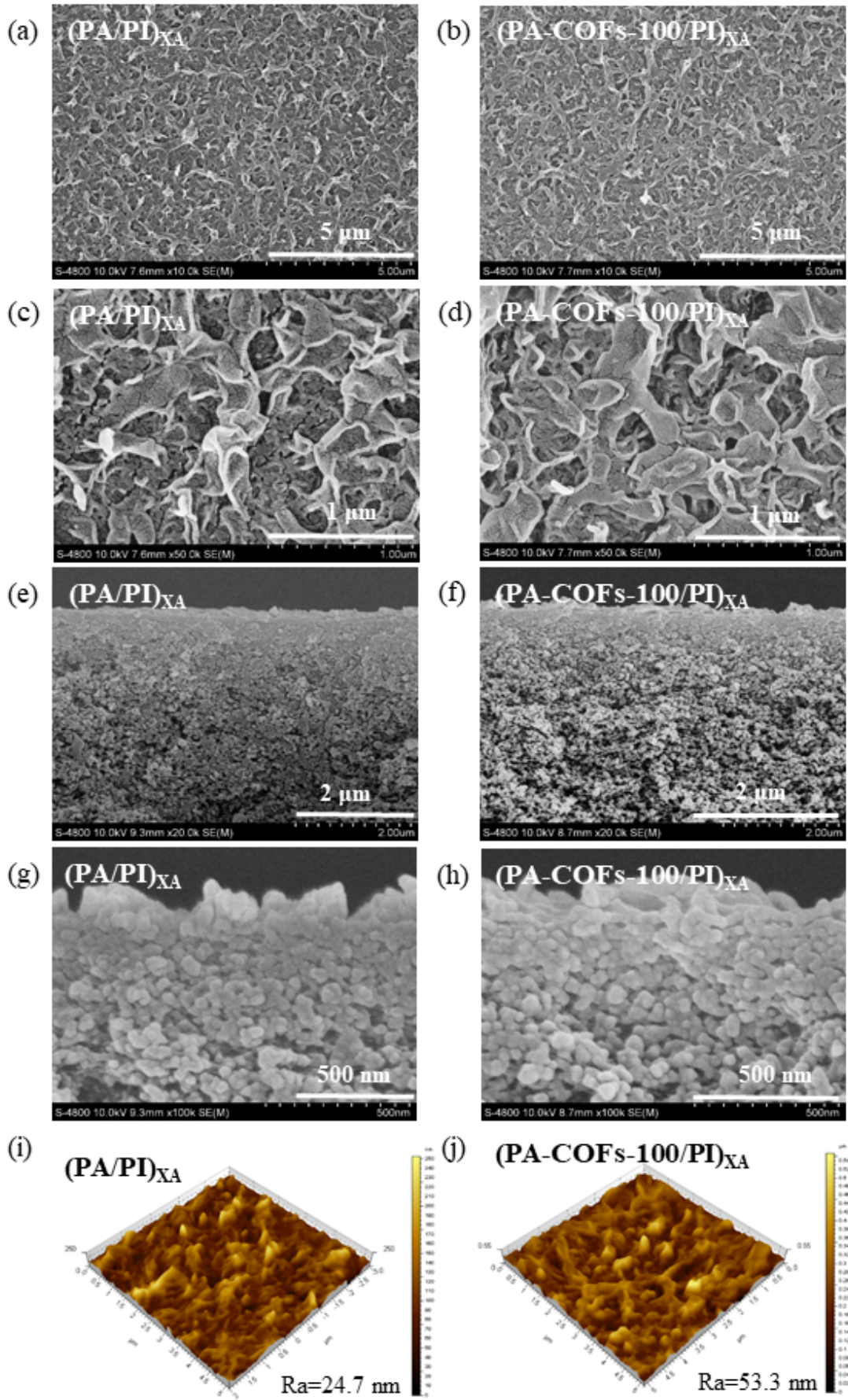
16 In addition, since the amount of SNW-1 added into the aqueous MPD solution is
17 relative low, and some of the IR absorption peaks of the SNW-1 nanoparticles
18 overlapped with the peaks which were attributed to the amide, imide or other groups of
19 the membrane polymers, the detection of the SNW-1 nanoparticles in the membrane
20 using ATR-FTIR was much challenging. For example, a broad band that appeared at
21 around $3000\text{-}3600\text{ cm}^{-1}$ was observed on the spectra of the $(\text{PA/PI})_{XA}$ and the $(\text{PA-}$
22 $\text{COFs-100/PI})_{XA}$ membranes, as illustrated in **Fig. S3**. This band might be assigned to

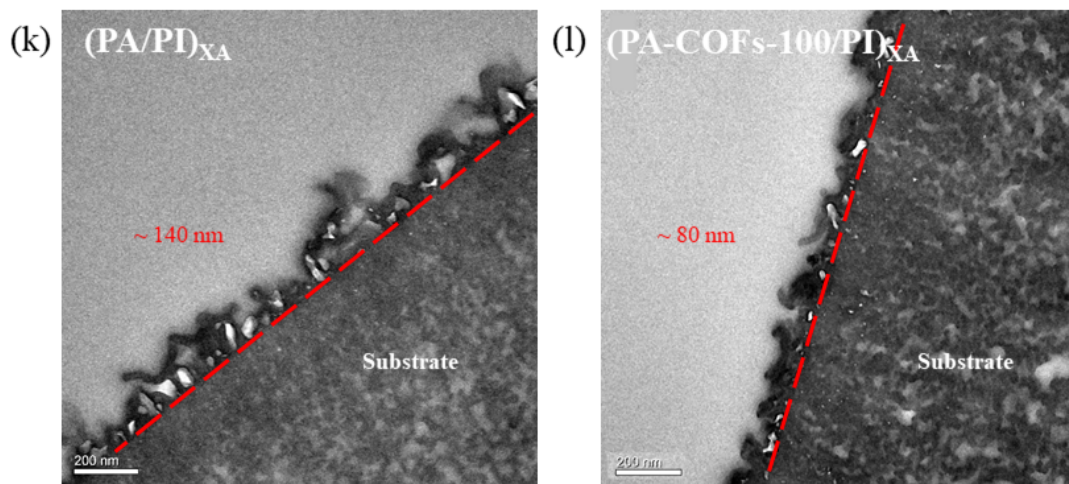
1 the combination of the N-H stretching vibration of SNW-1 nanoparticles, the N-H of
2 amide groups or the -OH stretching vibration of the carboxylic acid groups on the
3 membrane polymers [50]. Therefore, there is no significant difference in the ATR-FTIR
4 spectra between the TFN [(PA-COFs-100/PI)_{XA}] membrane and the TFC [(PA/PI)_{XA}]
5 membrane, as shown in **Fig. 3**.

6 XPS analysis provided a more sensitive technique to determine the surface
7 elemental composition of the OSN membrane and also to assess the existence of the
8 SNW-1 nanoparticles in the membrane top skin layer. **Table S1** summarized the atomic
9 concentration of the membrane surfaces with respect to carbon, nitrogen and oxygen.
10 As can be seen, the content percentage of the nitrogen element increased for the (PA-
11 COFs-100/PI)_{XA} membrane as compared with that of the (PA/PI)_{XA} membrane,
12 confirming the successful incorporation of the SNW-1 nanoparticles into the PA layer
13 [30]. **Error! Reference source not found.** presented the XPS spectra of N1s and O1s
14 for the (PA/PI)_{XA} and the (PA-COFs-100/PI)_{XA} membranes. On the N1s high-resolution
15 spectra, the (PA/PI)_{XA} membrane showed two peaks, which were corresponding to C-
16 NH₂ at 398.5 eV and O=C-NH at 399.1 eV [51, 52], respectively. However, a new peak
17 at 400.0 eV was observed for the (PA-COFs-100/PI)_{XA} membrane, as shown in **Error!**
18 **Reference source not found.** (b), which was assigned to the C=N-C bond of the SNW-
19 1 nanoparticles, indicating that the SNW-1 nanoparticles existed in the thin PA layer.
20 Additionally, the fractions of the carboxylic acid groups (O-C=O) and the unreacted
21 amine groups (C-NH₂) in the PA active layer increased with the incorporation of the
22 SNW-1 nanoparticles compared with that of the COFs-free TFC membrane, as shown

1 in **Fig. S4** (b) and (d), as well as in **Table S2**, which revealed that the SNW-1
2 nanoparticles incorporation slightly lowered the crosslinking degree of the PA layer
3 [53]. Similar results were also observed by Wang et al. [54] during their research works
4 of ZIF-8 nanoparticle-templated NF membranes for desalination. This suggested that
5 SNW-1 incorporation restricted the crosslinking reaction between MPD and TMC [39],
6 which might be due to the competition between SNW-1 and MPD, since it is known to
7 us that SNW-1 has secondary amine groups which can also react with TMC.

8 The effect of the SNW-1 incorporation on the surface morphology of the prepared
9 membranes was characterized through SEM, AFM and TEM analysis (**Fig. 4**). It could
10 be seen that the membrane surface showed a typical ridge and valley morphology, as
11 shown in **Fig. 4** (a)-(d). However, there are some difference between the TFC and the
12 TFN membranes. The “leaf-like” structures and high-density large bumps on the (PA-
13 COFs-100/PI)_{XA} TFN membrane surface were less obviously observed than those of
14 the (PA/PI)_{XA} TFC membrane surface, suggesting that the existence of the SNW-1
15 nanoparticles reduced the diffusion rate of the aqueous MPD and thus slowed down the
16 IP reaction rate [54]. The SEM images shown in **Fig. 4** (e)-(h) revealed that the addition
17 of the SNW-1 nanoparticles has little effect on the cross-sectional morphology of the
18 membrane and indicated a uniform dispersion of the SNW-1 nanoparticles within the
19 PA skin layer because of the good compatibility between the SNW-1 nanoparticles and
20 the PA polymer matrix of the skin layer.





1

2

3

4

5

6

7

8

9

10

11

12

13

14

15

16

17

Fig. 4. Surface SEM images, cross-sectional SEM images, AFM images and TEM images of (a, c, e, g, i, k) $(PA/PI)_{XA}$ TFC membrane and (b, d, f, h, j, l) $(PA-COFs-100/PI)_{XA}$ TFN membrane.

The surface morphologies of the OSN membranes were also characterized by AFM, as shown in **Fig. 4** (i) and (j). The top layer of the $(PA-COFs-100/PI)_{XA}$ membrane exhibited an increased surface roughness (53.3 nm) compared with that of the $(PA/PI)_{XA}$ membrane (24.7 nm), suggesting that the incorporation of the SNW-1 nanoparticles influenced the top-layer formation considerably. The much rougher surface indicated a higher specific surface area which was beneficial for solvents permeation [16].

TEM cross-sectional images of the $(PA/PI)_{XA}$ and $(PA-COFs-100/PI)_{XA}$ membranes are presented in **Fig. 4** (k) and (l). A PA top-layer was formed by the IP reaction on each substrate of the pristine $(PA/PI)_{XA}$ membrane and the hybrid $(PA-COFs-100/PI)_{XA}$ membrane, with thickness of ~140 nm for the former and ~80 nm for the latter, respectively. Much thinner PA active layer was obtained with the introduction

1 of the SNW-1 nanoparticles, which could facilitate the solvent transport. The PA layer
2 of the TFN membrane showed a less obviously protruding structure than that of the
3 TFC membrane, in coincident with the SEM morphology. The variation of the
4 morphology after the SNW-1 incorporation proved the effect of the hindrance of SNW-
5 1 on the diffusion of MPD molecules [21, 55].

6

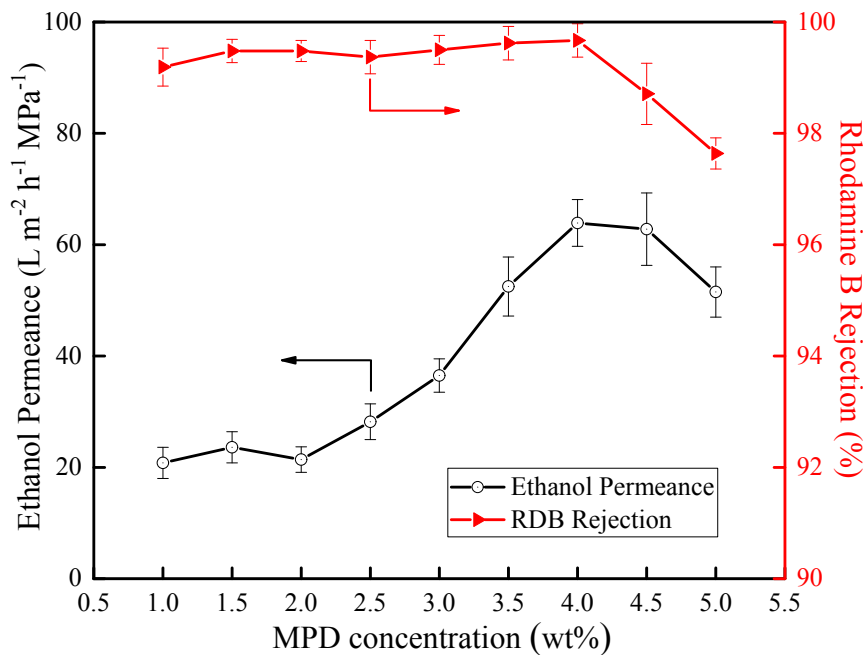
7 **3.3. Effects of fabrication conditions on membrane performance**

8 **3.3.1. Effect of MPD concentration**

9 As ethanol is commonly used to extract water-soluble pharmaceuticals [1] and is
10 an ideal solvent for OSN test [56], we selected RDB-ethanol solution to test the
11 separation performance of the prepared OSN membranes. **Fig. 5** shows the influence of
12 the MPD concentration on the separation performance of the TFN membranes, where
13 100 mg L^{-1} SNW-1 nanoparticles was added into the aqueous MPD solution and the
14 concentration of the TMC n-hexane solution was fixed at 0.15 wt%. The ethanol
15 permeance increased obviously while the RDB rejection varied only slightly as the
16 MPD concentration in the aqueous solution increased from 1.0 wt% to 4.0 wt%.

17 The change of the ethanol permeance is caused by the combined effects of the
18 surface roughness, membrane thickness and hydrophilicity. Generally speaking, higher
19 surface roughness is beneficial for the solvent permeation. However, reduced
20 hydrophilicity and increased membrane thickness can hinder the effective solvent
21 transport and result in a decreased ethanol permeance [57]. When the MPD
22 concentration is increased from 1.0 wt% to 4.0 wt%, the larger surface area and the

1 crumpling phenomenon that could occur due to the higher rate of the interfacial
 2 reactions with the increase of the aqueous monomer concentration [58], thus the surface
 3 roughness is dramatically increased. Theoretically, higher MPD concentration leads to
 4 less unreacted -COCl groups and thicker active layer, thus the hydrophilicity of the
 5 membrane decreases and the solvent penetration resistance increases, which has
 6 adverse impact on the ethanol permeance [57, 59]. The positive effect for improving
 7 solvent permeance by the increased surface roughness offsets the negative effect of both
 8 the less-hydrophilic surface and the appropriately increased membrane thickness with
 9 the increased MPD concentration, consequently resulting in an enhancement in the
 10 ethanol permeance.



11
 12 **Fig. 5.** Effect of MPD concentration on the membrane performance. (SNW-1 content:
 13 $100 mg L^{-1}$, TMC concentration: 0.15 wt%)

14
 15 However, both the permeance and the rejection decreased when the MPD

1 concentration was further increased higher than 4.0 wt% (i.e., 4.5 wt% and 5.0 wt% in
2 **Fig. 5**). Under such circumstances, more acyl chloride groups from TMC reacted with
3 MPD to form a relatively hydrophobic and thick PA film, thus decreased the solvent
4 permeance [57]. Moreover, the high MPD/TMC molar ratio could not allow to form a
5 uniform and dense selective skin layer across the membrane surface due to the lack of
6 sufficient TMC [60]. Therefore, the RDB rejection of the OSN membrane prepared at
7 high MPD concentration was relatively low.

8 For the preparation of conventional COFs-free TFC OSN membranes, 2.0 wt%
9 was selected as the routine MPD concentration of the aqueous monomer solution to
10 obtain an excellent separation performance [10]. However, when the SNW-1
11 nanoparticles were incorporated, our experiment results showed that a higher MPD
12 concentration was necessary, especially for better ethanol permeance. It suggested that
13 when SNW-1 existed during the IP reaction, the nanoparticles might provide a mass
14 transfer resistance to the diffusion of the aqueous monomer and thus affect the reaction
15 between diamine and acyl chloride group [21]. Therefore, a higher MPD concentration
16 was needed to form TFN OSN membranes with higher ethanol permeance in the
17 presence of SNW-1. As a result, 4.0 wt% was determined as the optimal aqueous MPD
18 concentration and was applied in the subsequent experimental studies.

19 **3.3.2. Effect of TMC concentration**

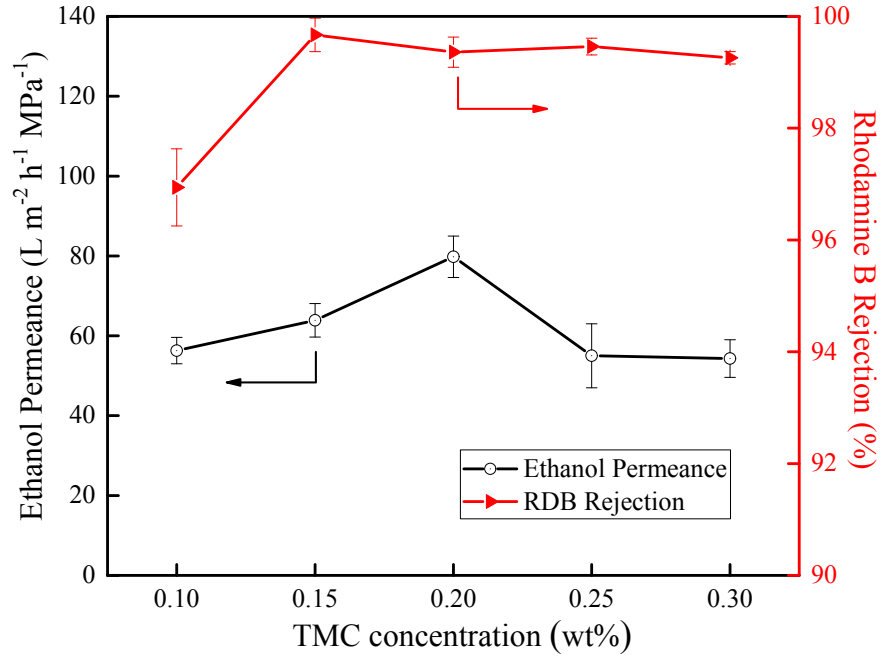
20 The effect of TMC concentration on the membrane separation performance can be
21 seen from **Fig. 6**. Both the RDB rejection and the ethanol permeance increased
22 apparently when the TMC concentration increased from 0.10 to 0.20 wt%. With respect

1 to the rejection, it was suggested that membranes with increased thickness, compactness,
2 and higher crosslinking degree in the skin layer could be obtained with the increase of
3 the TMC concentration [57], and thus provide higher solute rejection.

4 Generally, relative high TMC concentration could result in a larger amount of
5 unreacted -COCl groups which could easily become -COOH after hydration, thus
6 increasing the membrane hydrophilicity [59]. Meanwhile, at relative high TMC
7 concentration, it is common to us that the reaction rate between TMC and the secondary
8 amine of SNW-1 was faster and the incorporation effect of SNW-1 was surely better,
9 which could help prevail over the effect of the PA active layer from MPD and TMC
10 [21, 57]. Thus, the higher TMC concentration resulted in an improved hydrophilicity
11 and further an increased solvent passage caused by the multiporous structure of SNW-
12 1. This suggested that the positive effects of the enhanced membrane hydrophilicity
13 could overcome the negative effects of the thicker and denser membrane structure on
14 the solvent permeability when TMC concentration was below 0.20 wt%. Therefore, the
15 observed ethanol permeance increased in this TMC concentration range, as can be seen
16 from **Fig. 6**.

17 However, when the TMC concentration increased further from 0.20 wt% up to
18 0.30 wt%, the ethanol permeance reduced significantly, from $79.8 \text{ L m}^{-2} \text{ h}^{-1}$
19 MPa^{-1} , indicating that the increase of the membrane thickness caused by the higher
20 TMC concentration could induce more mass transfer resistance to the solvent [61].
21 Nevertheless, the RDB rejection was almost constant at around 99.3%. Consequently,
22 0.20 wt% was selected as the optimal TMC concentration considering both the

1 performance of the ethanol permeance and the RDB rejection.



2

3 **Fig. 6.** Effect of TMC concentration on the membrane performance. (MPD

4 concentration: 4.0 wt%, SNW-1 content: 100 mg L⁻¹)

5

6 3.3.3. Effect of SNW-1 incorporation

7 The effect of the SNW-1 nanoparticles incorporation in the aqueous MPD solution

8 on the separation performance of the TFN OSN membranes is shown in **Fig. 7.** The

9 ethanol permeance increased from 54.4 L m⁻² h⁻¹ MPa⁻¹ (for the conventional COFs-

10 free TFC membrane) to 79.8 L m⁻² h⁻¹ MPa⁻¹ (for the TFN membrane with 100.0 mg

11 L⁻¹ SNW-1 incorporated), with an enhancement of 46.7%. However, with the further

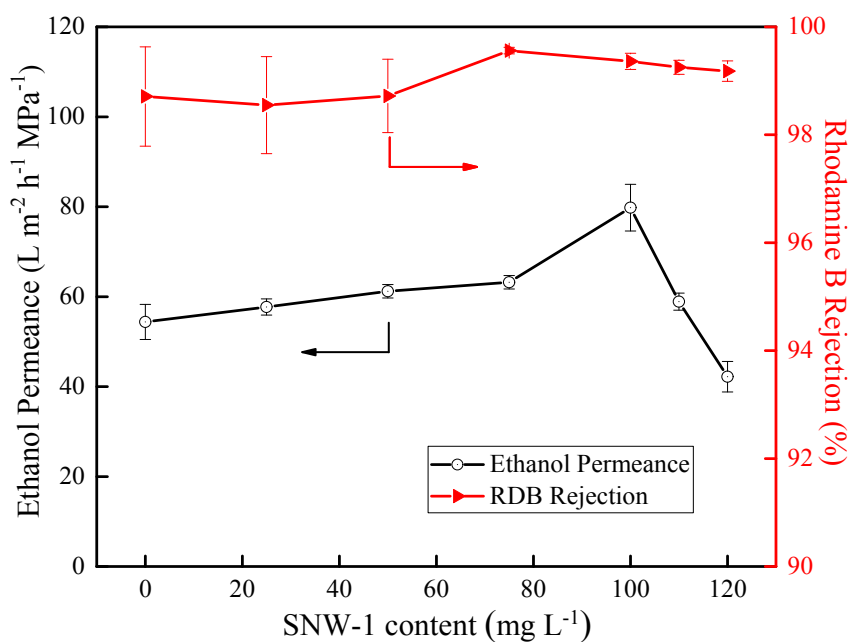
12 increase of the SNW-1 loading, the ethanol permeance decreased gradually. The RDB

13 rejection showed a similar trend. It increased from 98.5% up to 99.6% as the SNW-1

14 loading increased from 20.0 to 75.0 mg L⁻¹, and subsequently showed a slight decrease

15 to 99.2% at even higher loading up to 120 mg L⁻¹, indicating that the SNW-1 loading

1 amount has minor effect on the solute rejection. At 100 mg L⁻¹ SNW-1 loading, the
2 prepared membrane showed the best separation performance in both ethanol permeance
3 (79.8 L m⁻² h⁻¹ MPa⁻¹) and RDB rejection (99.4%), which effectively overcame the
4 trade-off paradox between the solvent permeance and the solute rejection.



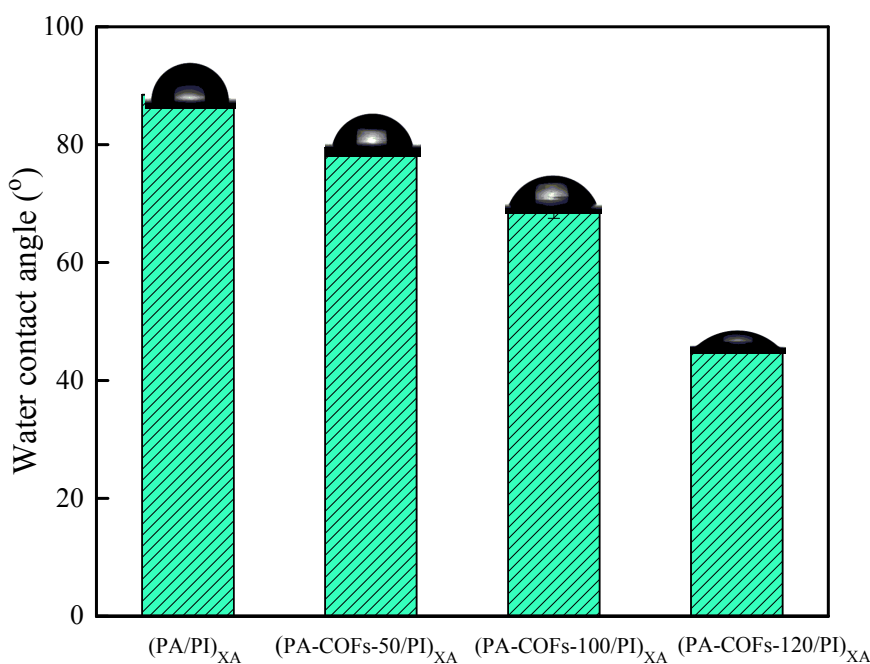
5

6 **Fig. 7.** Effect of the SNW-1 content on the TFN OSN membrane performance. (MPD
7 concentration: 4.0 wt%, TMC concentration: 0.20 wt%)

8

9 Results here clearly demonstrated that the SNW-1 nanoparticles made a great
10 contribution to the significant enhancement of the ethanol permeance, while
11 maintaining the dye rejection. The increase in solvent permeance of the OSN
12 membranes could be attributed to several factors. First, the transport of polar solvents
13 such as ethanol is improved with the enhanced hydrophilicity [62], as the water contact
14 angles declined with the increase of the SNW-1 loadings (**Fig. 8**). The pores of the
15 SNW-1 nanoparticles dispersing in the PA skin layer could provide additional channels

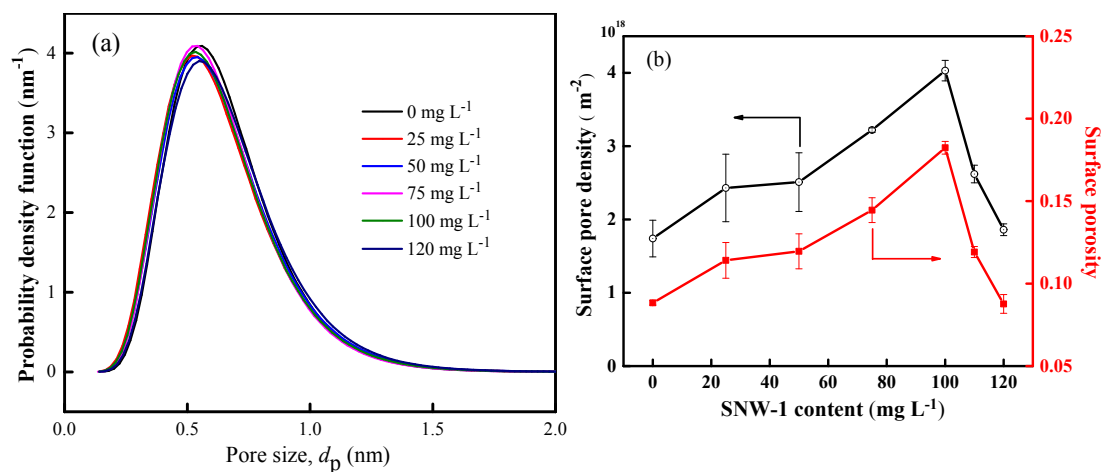
1 to allow the permeation of the ethanol molecules [30]. Moreover, the incorporated
2 SNW-1 led to a lower crosslinking degree of the polymer matrix at the interfacial region
3 between SNW-1 and the polyamide matrix [19], thus both the pore density and the
4 porosity of the skin layer increased, as shown in **Fig. S4**, **Fig. 9** and **Table S3**. Finally,
5 the (PA-COFs-100/PI)_{XA} membranes showed more rough surface and thinner PA
6 selective layer thickness than the COFs-free TFC membrane (**Fig. 4**), which resulted in
7 low-resistance pathways for ethanol molecules to penetrate through the PA skin layer
8 [63].



9
10 **Fig. 8.** Contact angles of the prepared TFN membrane surfaces with different content
11 of the SNW-1 nanoparticles incorporated.

12
13 When the SNW-1 nanoparticles loading was in the range of 25 to 100.0 mg L⁻¹,
14 the obtained TFN OSN membranes had similar average pore size and probability
15 density function curve (**Fig. 9 (a)**), as well as an increased surface porosity (**Fig. 9 (b)**)

1 and **Table S3**). Therefore, the prepared membrane had relative higher ethanol
2 permeance with no compromise of the solute rejection, as shown in **Fig. 7**, indicating
3 the good compatibility between the SNW-1 nanoparticles and the PA active layer
4 because of the covalent bonding between the SNW-1 nanoparticles and the backbone
5 of the PA active layer.



6
7 **Fig. 9.** Probability density function curves of the pore size (a), and the surface pore
8 density and surface porosity (b) of the membranes with the incorporated SNW-1
9 content.

10
11 However, a further increase in SNW-1 loading beyond 100 mg L^{-1} resulted in a
12 distinct reduction of the ethanol permeance. This could be ascribed to the fact that a
13 higher SNW-1 content might take up more space from the PA selective layer, which
14 would result in a relatively thicker selective layer compared with that of the TFC
15 membrane [19], consequently a more hydrodynamic resistance. Furthermore, the
16 restrained chain mobility in the active layer due to the SNW-1 incorporation would
17 weaken the mobility of the polymer chains and also slow down the solvent penetration

1 [64]. Thus, the ethanol permeance dropped distinctly.

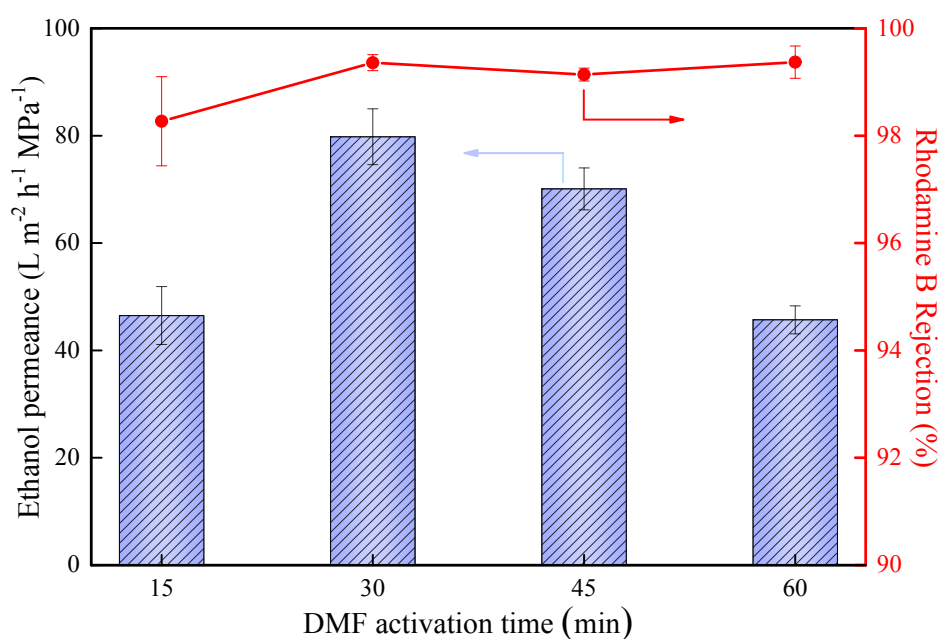
2 Overall, the SNW-1 incorporation does not influence the RDB rejection greatly.
3 However, the solute rejection decreased quite slightly as the SNW-1 loading increased
4 from 75.0 to 120.0 mg L⁻¹. The decreased solute rejection might be attributed to the
5 competition between MPD and the SNW-1 nanoparticles which interfered the main IP
6 reaction between MPD and TMC, and reduced the crosslinking degree of the PA
7 polymers in the matrix of the (PA-COFs/PI)_{XA} membranes [54]. These phenomena were
8 even apparently at higher SNW-1 nanoparticles content and resulted in facilitating the
9 passage of solutes. Further, the reduced solvent permeance increased the solute
10 concentration in the permeate. Thus, the Rhodamine B rejection decreased slightly.

11 **3.3.4. Effect of the solvent activation time with DMF**

12 It was proven earlier that solvent activation remarkably promotes the permeance
13 of TFC OSN membranes without compromising retention [5, 10, 65]. In this work,
14 DMF was chosen as the activating solvent to investigate the influence of the solvent
15 immersion time. The surface and cross-sectional morphologies of the (PA-COFs-
16 100/PI)_{XA} membrane with DMF activation time were characterized by SEM (**Fig. S5**).
17 No distinct differences could be observed among the morphologies of the TFN OSN
18 membranes with different DMF activation time, indicating that the activation process
19 had little influence on the overall morphologies of the TFN membranes.

20 As shown in **Fig. 10**, the separation performance of the TFN OSN membranes was
21 significantly promoted by increasing the DMF immersion time up to 30 min, indicating
22 that the solvent activation can cause a temporary swelling of the top skin layer, so that

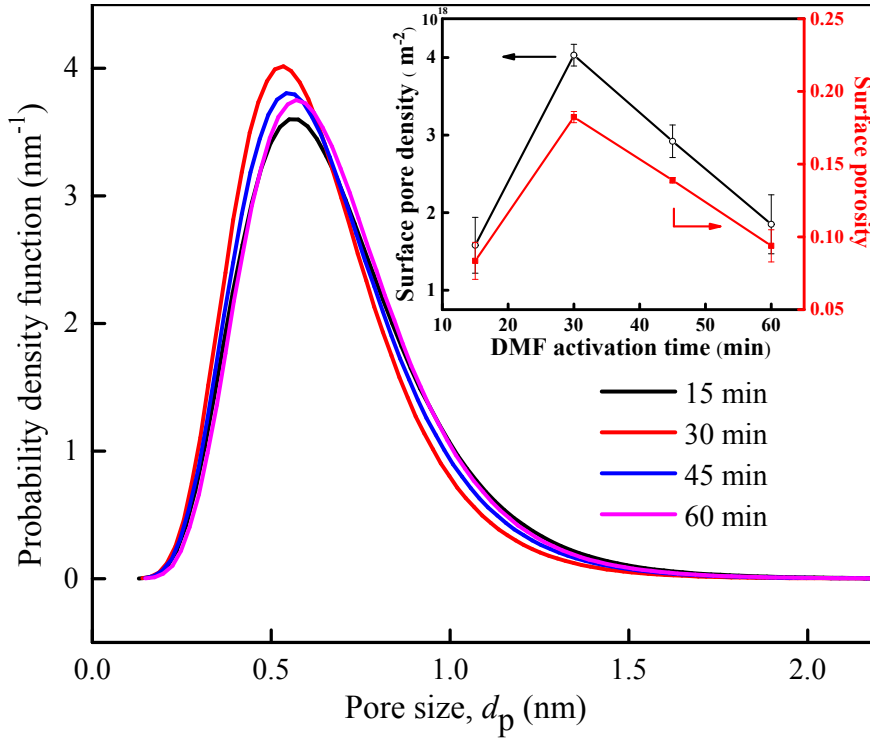
1 some PA oligomer fragments with low molecular weight would dissolve in the
2 activating solvent and additional free volume (previously blocked by these low
3 molecular weight PA fragments) would be created in the top skin layer [10, 66]. Thus,
4 both the pore density and the porosity increased, as shown in **Fig. 11** and **Table S4**,
5 which resulted in a higher permeance. Furthermore, the imperfections or defects in the
6 top skin layer were removed because of the annealing effects during the swelling
7 operation [10], and thus a denser membrane skin layer was formed, so that the peaks of
8 the probability density function curve of the pore size in the skin layer became higher
9 and the average pore size shifted smaller (**Fig. 11**), resulting in an increased rejection.



10
11 **Fig. 10.** Effect of DMF activation time on the membrane performance.

12
13 However, a further increase of the immersion time from 30 min resulted in a
14 decreased ethanol permeance because of the relative small pore density and porosity
15 (**Fig. 11** and **Table S4**) caused by the densification effect which occurred when the

1 membrane sample was immersed for a further longer time in DMF [67].



2

3 **Fig. 11.** Probability density function of the pore size (d_p) and the surface pore density
4 and the surface porosity of the (PA-COFs-100/PI)_{XA} membranes with the DMF
5 activation time.

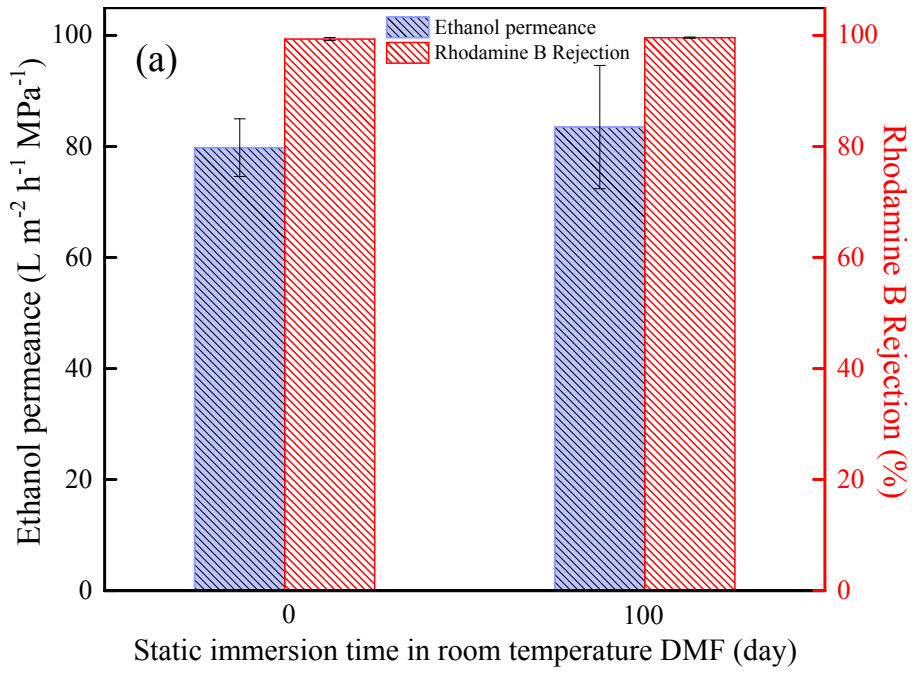
6

7 **3.4. Long-term performance tests of the TFN membrane**

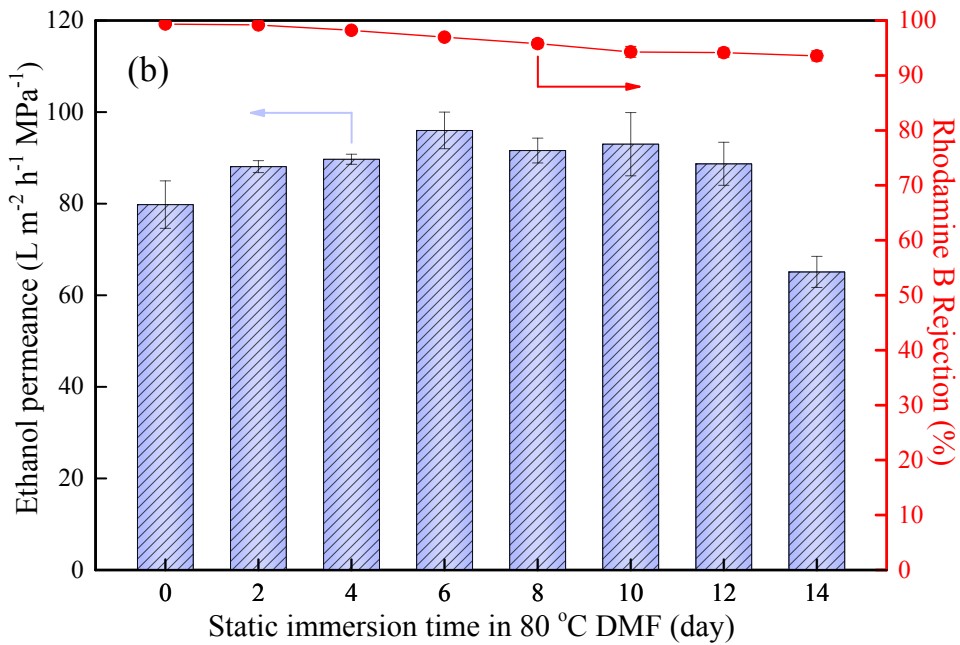
8 The (PA-COFs-100/PI)_{XA} membranes with 30-min DMF activation were chosen
9 to perform an extending immersion test to investigate their long-term stability in DMF
10 under different temperature.

11 After being static immersed in DMF at room temperature for 100 days, as can be
12 seen from **Fig. 12 (a)** **Error! Reference source not found.**, the ethanol permeance
13 increased from 79.8 L m⁻² h⁻¹ MPa⁻¹ up to 83.5 L m⁻² h⁻¹ MPa⁻¹ and the RDB rejection
14 remained up to 99.0%, indicating that the COFs-incorporated TFN membranes owned

1 remarkable solvent resistance.



2
3



4

5 **Fig. 12.** The long-term performance test of the $(\text{PA-COFs-100/PI})_{\text{XA}}$ membranes after
6 persistent static immersion in DMF (a) at room temperature for 100 days, and (b) at
7 80 °C within 14 days.

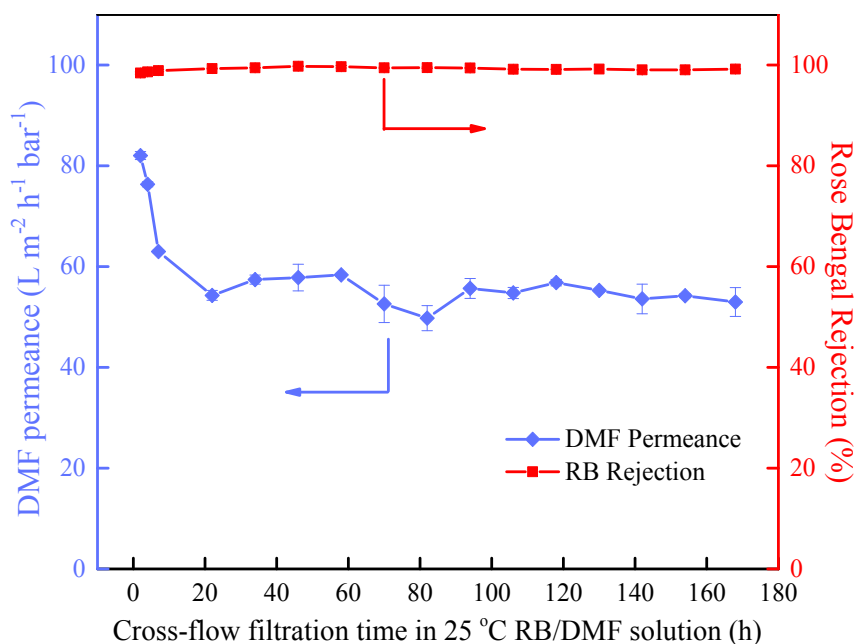
8

1 In order to accelerate the solvent resistance test, the prepared OSN membranes
2 were statically immersed in DMF at 80 °C over 14 days and were taken out periodically
3 to test the separation performance, as shown in **Fig. 12 (b)**. The ethanol permeance
4 slightly increased and the RDB rejection slightly decreased during the initial 6 days.
5 An ethanol permeance of 96.0 L m⁻² h⁻¹ MPa⁻¹ and a RDB rejections of above 97%
6 were achieved at the end of the 6 day's static immersion (**Fig. 12 (b)**). However, the
7 rejection decreased continuously, together with the decrease of the permeance with the
8 further elongation of the static immersion time to 14 days.

9 The chemical and morphological structure changes of the (PA-COFs-100/PI)_{XA}
10 membranes after being immersed in DMF at 80 °C for 14 days were characterized by
11 ATR-FTIR and SEM, as presented in **Fig. S6** and **Fig. S7**. According to the ATR-FTIR
12 spectra, the characteristic peaks of the imide groups increased obviously and the amide
13 groups diminished significantly, indicating that the long-term high temperature
14 immersion in solvent caused the reversing trend in membrane chemical structure. The
15 integral “leaf-like” structures and high-density large bumps were also suffered
16 somehow destruction. Both the above chemical and morphological structure changes
17 explained the decreased RDB rejection. Additionally, the reduction of the ethanol
18 permeance can be attributed to the fact that the persistent solvent exposure at high
19 temperature resulted in the reduced surface protuberance because of the persistent
20 annealing effect caused by DMF [67] after 14 day's high temperature immersion.

21 Besides the long-term static immersion test in DMF under different temperature
22 for different time, we further conducted a long-term (7 days) continuous cross-flow

1 filtration test using 100 mg L^{-1} Rose Bengal (1017 Da) DMF solution at $25 \text{ }^{\circ}\text{C}$ to
2 investigate the solvent resistance of the prepared OSN membranes, as shown in **Fig. 13**.



3
4 **Fig. 13.** The long-term filtration performance of the $(\text{PA-COFs-100/PI})_{\text{XA}}$ membranes
5 using 100 mg L^{-1} Rose Bengal (1017 Da) DMF solution at $25 \text{ }^{\circ}\text{C}$.
6

7 As can be seen from **Fig. 13**, the RB rejection kept at $99.5 \pm 0.3\%$ during the 7 days'
8 continuous cross-flow filtration in RB/DMF solution at $25 \text{ }^{\circ}\text{C}$, indicating that the
9 prepared $(\text{PA-COFs-100/PI})_{\text{XA}}$ membranes exhibited excellent solvent resistance. The
10 gradual decrease in DMF permeance during the first 22 h might be due to the membrane
11 fouling. However, the DMF permeance could maintain a relative constant value of
12 about $55.0 \text{ L m}^{-2} \text{ h}^{-1} \text{ MPa}^{-1}$, indicating the excellent application potential of the COFs-
13 incorporated OSN membrane we prepared in strong polar organic solvents.
14

15 **3.5. The performance comparison of the TFN membrane with the state-of-the-art**
16 **data**

1 **Error! Reference source not found.** benchmarks the separation performance of
2 our new COFs-incorporated TFN membranes in comparison with those of the state-of-
3 the-art OSN membranes reported in the literatures. For comparison, only those OSN
4 membranes tested using ethanol-solute solution were selected. It can be seen that our
5 (PA-COFs/PI)_{XA} membranes showed overall high solvent permeances with excellent
6 solute rejections compared with other literature OSN membranes. Among the
7 exceptions, a few of the reported membranes (named as TiO₂/Ppy, PEI-sPPSU,
8 MWCNTs-COOH/P84 MMM) have relative higher ethanol permeance, however, they
9 all have relative lower solution rejection.

10 Comparing to those 99+% high rejection membranes, our membranes provide the
11 highest ethanol permeance (79.8 L m⁻² h⁻¹ MPa⁻¹). Moreover, this kind of COFs-
12 incorporated TFN membranes have remarkable solvent resistance according to the
13 long-term static immersion test in DMF at room temperature for 100 days, which is
14 much promising for commercial OSN applications.

15

16 **4. Conclusion**

17 A class of novel TFN OSN membranes were successfully synthesized by a
18 modified IP reaction between SNW-1 (COFs) nanoparticles-incorporated aqueous
19 MPD solution and TMC hexane solution on the PI substrate, followed by chemical
20 crosslinking and solvent DMF activation. The improved hydrophilicity of the TFN
21 membrane surface, the rougher membrane surface structure, and the thinner PA skin
22 layer all contributed to the enhancement of the solvent (ethanol) permeance which was

1 up to 46.7%. The ethanol permeance reached $79.8 \text{ L m}^{-2} \text{ h}^{-1} \text{ MPa}^{-1}$ at a 99.4% rejection
2 of RDB (479 Da). In addition, as the SNW-1 nanoparticles was covalently linked to the
3 PA active layer, the prepared TFN OSN membranes demonstrated excellent solvent
4 resistance according to the long-term static immersion in DMF at room temperature for
5 100 days and the continuous cross-flow filtration of RB/DMF solution at 25 °C for 7
6 days, as well as the statically high-temperature immersion in DMF at 80 °C for 14 days,
7 indicating a promising prospective in OSN applications.

8

9 **Acknowledgements**

10 This work was supported by National Natural Science Foundation of China (No.
11 21476218), the Fundamental Research Funds for the Central Universities of China (No.
12 201822012). This is MCTL Contribution No.182. The authors would give great thanks
13 to Dr. Prof. W. S. Winston Ho for his kind guide and Dr. Dongzhu Wu for his kind help
14 when Dr. Prof Baowei Su worked as a visiting scholar in The Ohio State University
15 during Nov. 2016 - Nov. 2017. Dr. Michael Z. Hu' research effort to prepare this paper
16 is partially sponsored by the U.S. Department of Energy, Bioenergy Technologies
17 Office (WBS 2.5.5.507).

18

19 **Nomenclature**

20 A —Membrane area, m^2

21 Δt —Time, h

22 Δp —Transmembrane pressure, MPa

- 1 ΔV —Volume permeated, L
- 2 P —Solvent permeance, $\text{L m}^{-2} \text{h}^{-1} \text{MPa}^{-1}$
- 3 R —Solute rejection, %
- 4 C_p —Concentration of solute in the permeate, mg L^{-1}
- 5 C_f —Concentration of solute in the feed, mg L^{-1}
- 6 $f_R(r)$ —Log-normal probability density function, m^{-1}
- 7 b —Parameter defined by Eq. (3), dimensionless
- 8 r —Membrane pore radius, m
- 9 Greek letter
- 10 r^* —Mean pore radius, m
- 11 σ^* —Distribution standard deviation, m
- 12 ρ —Pore density, m^{-2}
- 13 ε —Surface porosity, -

14

15 **References**

- 16 [1] P. Marchetti, M.F. Jimenez Solomon, G. Szekely, A.G. Livingston, Molecular
 17 separation with organic solvent nanofiltration: a critical review, *Chem. Rev.* 114 (2014)
 18 10735-10806.
- 19 [2] P. Vandezande, L.E. Gevers, I.F. Vankelecom, Solvent resistant nanofiltration:
 20 separating on a molecular level, *Chem. Soc. Rev.* 37 (2008) 365-405.
- 21 [3] S. Hermans, H. Mariën, C. Van Goethem, I.F.J. Vankelecom, Recent developments
 22 in thin film (nano)composite membranes for solvent resistant nanofiltration, *Curr. Opin.*
 23 *Chem. Eng.* 8 (2015) 45-54.
- 24 [4] S.K. Lim, K. Goh, T.-H. Bae, R. Wang, Polymer-based membranes for solvent-
 25 resistant nanofiltration: A review, *Chinese J. Chem. Eng.* (2017).
- 26 [5] M.F. Jimenez Solomon, Y. Bhole, A.G. Livingston, High flux hydrophobic
 27 membranes for organic solvent nanofiltration (OSN)—Interfacial polymerization,
 28 surface modification and solvent activation, *J. Membr. Sci.* 434 (2013) 193-203.
- 29 [6] S. Tsarkov, V. Khotimskiy, P.M. Budd, V. Volkov, J. Kukushkina, A. Volkov,
 30 Solvent nanofiltration through high permeability glassy polymers: Effect of polymer

- 1 and solute nature, *J. Membr. Sci.* 423-424 (2012) 65-72.
- 2 [7] J. Campbell, J.D.S. Burgal, G. Szekely, R.P. Davies, D.C. Braddock, A. Livingston,
3 Hybrid polymer/MOF membranes for Organic Solvent Nanofiltration (OSN): Chemical
4 modification and the quest for perfection, *J. Membr. Sci.* 503 (2016) 166-176.
- 5 [8] F. Fei, L. Cseri, G. Szekely, C.F. Blanford, Robust Covalently Cross-linked
6 Polybenzimidazole/Graphene Oxide Membranes for High-Flux Organic Solvent
7 Nanofiltration, *ACS Appl. Mater. Interfaces* 10 (2018) 16140-16147.
- 8 [9] G. Szekely, M.F. Jimenez-Solomon, P. Marchetti, J.F. Kim, A.G. Livingston,
9 Sustainability assessment of organic solvent nanofiltration: from fabrication to
10 application, *Green Chem.* 16 (2014) 4440-4473.
- 11 [10] M.F. Jimenez Solomon, Y. Bhole, A.G. Livingston, High flux membranes for
12 organic solvent nanofiltration (OSN)—Interfacial polymerization with solvent
13 activation, *J. Membr. Sci.* 423-424 (2012) 371-382.
- 14 [11] M.H. Abdellah, L. Pérez-Manríquez, T. Puspasari, C.A. Scholes, S.E. Kentish, K.-
15 V. Peinemann, A catechin/cellulose composite membrane for organic solvent
16 nanofiltration, *J. Membr. Sci.* 567 (2018) 139-145.
- 17 [12] L.P. Patrizia Marchetti, and Andrew Livingston, The Selectivity Challenge in
18 Organic Solvent Nanofiltration: Membrane and Process Solutions, *Annu. Rev. Chem.*
19 *Biomol. Eng.* 8 (2017) 21.21–21.25.
- 20 [13] S.-P. Sun, T.-S. Chung, K.-J. Lu, S.-Y. Chan, Enhancement of flux and solvent
21 stability of Matrimid®-thin-film composite membranes for organic solvent
22 nanofiltration, *AIChE J.* 60 (2014) 3623-3633.
- 23 [14] Y. Li, L.H. Wee, J.A. Martens, I.F.J. Vankelecom, Interfacial synthesis of ZIF-8
24 membranes with improved nanofiltration performance, *J. Membr. Sci.* 523 (2017) 561-
25 566.
- 26 [15] Y. Li, H. Mao, H. Zhang, G. Yang, R. Ding, J. Wang, Tuning the microstructure
27 and permeation property of thin film nanocomposite membrane by functionalized
28 inorganic nanospheres for solvent resistant nanofiltration, *Sep. Purif. Technol.* 165
29 (2016) 60-70.
- 30 [16] M. Peyravi, M. Jahanshahi, A. Rahimpour, A. Javadi, S. Hajavi, Novel thin film
31 nanocomposite membranes incorporated with functionalized TiO₂ nanoparticles for
32 organic solvent nanofiltration, *Chem. Eng. J.* 241 (2014) 155-166.
- 33 [17] S. Sorribas, P. Gorgojo, C. Tellez, J. Coronas, A.G. Livingston, High flux thin film
34 nanocomposite membranes based on metal-organic frameworks for organic solvent
35 nanofiltration, *J. Am. Chem. Soc.* 135 (2013) 15201-15208.
- 36 [18] L. Huang, J. Chen, T. Gao, M. Zhang, Y. Li, L. Dai, L. Qu, G. Shi, Reduced
37 Graphene Oxide Membranes for Ultrafast Organic Solvent Nanofiltration, *Adv. Mater.*
38 28 (2016) 8669-8674.
- 39 [19] F.Y. Zhao, Y.L. Ji, X.D. Weng, Y.F. Mi, C.C. Ye, Q.F. An, C.J. Gao, High-Flux
40 Positively Charged Nanocomposite Nanofiltration Membranes Filled with
41 Poly(dopamine) Modified Multiwall Carbon Nanotubes, *ACS Appl. Mater. Inter.* 8
42 (2016) 6693-6700.
- 43 [20] X. Wu, L. Hao, J. Zhang, X. Zhang, J. Wang, J. Liu, Polymer-Ti₃C₂T_x
44 composite membranes to overcome the trade-off in solvent resistant nanofiltration for

1 alcohol-based system, *J. Membr. Sci.* 515 (2016) 175-188.

2 [21] H. Dong, L. Zhao, L. Zhang, H. Chen, C. Gao, W.S. Winston Ho, High-flux reverse
3 osmosis membranes incorporated with NaY zeolite nanoparticles for brackish water
4 desalination, *J. Membr. Sci.* 476 (2015) 373-383.

5 [22] Y. Zhang, R. Wang, Fabrication of novel polyetherimide-fluorinated silica
6 organic–inorganic composite hollow fiber membranes intended for membrane
7 contactor application, *J. Membr. Sci.* 443 (2013) 170-180.

8 [23] X. Guo, D. Liu, T. Han, H. Huang, Q. Yang, C. Zhong, Preparation of thin film
9 nanocomposite membranes with surface modified MOF for high flux organic solvent
10 nanofiltration, *AIChE J.* 63 (2017) 1303-1312.

11 [24] Z. Yuan, X. Wu, Y. Jiang, Y. Li, J. Huang, L. Hao, J. Zhang, J. Wang, Carbon
12 dots-incorporated composite membrane towards enhanced organic solvent
13 nanofiltration performance, *J. Membr. Sci.* 549 (2018) 1-11.

14 [25] C.S. Diercks, O.M. Yaghi, The atom, the molecule, and the covalent organic
15 framework, *Science* 355 (2017).

16 [26] S.Y. Ding, W. Wang, Covalent organic frameworks (COFs): from design to
17 applications, *Chem. Soc. Rev.* 42 (2013) 548-568.

18 [27] X. Zhuang, Y. Mai, D. Wu, F. Zhang, X. Feng, Two-dimensional soft
19 nanomaterials: a fascinating world of materials, *Adv. Mater.* 27 (2015) 403-427.

20 [28] X.D. X. Feng, D. Jiang, Covalent organic frameworks, *Chem. Soc. Rev.* 41 (2012)
21 6010–6022.

22 [29] L. Valentino, M. Matsumoto, W.R. Dichtel, B.J. Marinas, Development and
23 Performance Characterization of a Polyimine Covalent Organic Framework Thin-Film
24 Composite Nanofiltration Membrane, *Environ. Sci. Technol.* 51 (2017) 14352-14359.

25 [30] C. Wang, Z. Li, J. Chen, Z. Li, Y. Yin, L. Cao, Y. Zhong, H. Wu, Covalent organic
26 framework modified polyamide nanofiltration membrane with enhanced performance
27 for desalination, *J. Membr. Sci.* 523 (2017) 273-281.

28 [31] J.G. Hongwei Fan, Hong Meng, Alexander Knebel, and Jürgen Caro, High-Flux
29 Imine-Linked Covalent Organic Framework COF-LZU1 Membranes on Tubular
30 Alumina Supports for Highly Selective Dye Separation by Nanofiltration, *Angew.
31 Chem.* 130 (2018) 4147-4151.

32 [32] R. Wang, X. Shi, A. Xiao, W. Zhou, Y. Wang, Interfacial polymerization of
33 covalent organic frameworks (COFs) on polymeric substrates for molecular separations,
34 *J. Membr. Sci.* 566 (2018) 197-204.

35 [33] H. Yang, H. Wu, F. Pan, Z. Li, H. Ding, G. Liu, Z. Jiang, P. Zhang, X. Cao, B.
36 Wang, Highly water-permeable and stable hybrid membrane with asymmetric covalent
37 organic framework distribution, *J. Membr. Sci.* 520 (2016) 583-595.

38 [34] X. Wu, Z. Tian, S. Wang, D. Peng, L. Yang, Y. Wu, Q. Xin, H. Wu, Z. Jiang,
39 Mixed matrix membranes comprising polymers of intrinsic microporosity and covalent
40 organic framework for gas separation, *J. Membr. Sci.* 528 (2017) 273-283.

41 [35] X. Gao, X. Zou, H. Ma, S. Meng, G. Zhu, Highly selective and permeable porous
42 organic framework membrane for CO₂ capture, *Adv. Mater.* 26 (2014) 3644-3648.

43 [36] B.F. Matthias Georg Schwab, Hans Wolfgang Spiess, Arne Thomas, Xinliang
44 Feng, and Klaus Mullen, Catalyst-free Preparation of Melamine-Based Microporous

1 Polymer Networks through Schiff Base Chemistry, *J. Am. Chem. Soc.* 131 (2009)
2 7216-7217.

3 [37] J. Chau, P. Basak, K.K. Sirkar, Reverse osmosis separation of particular organic
4 solvent mixtures by a perfluorodioxole copolymer membrane, *J. Membr. Sci.* (2018).

5 [38] M.H. Davood Abadi Farahani, T.-S. Chung, Solvent resistant hollow fiber
6 membranes comprising P84 polyimide and amine-functionalized carbon nanotubes
7 with potential applications in pharmaceutical, food, and petrochemical industries,
8 *Chem. Eng. J.* 345 (2018) 174-185.

9 [39] C. Li, S. Li, L. Lv, B. Su, M.Z. Hu, High Solvent-resistant and Integrally
10 Crosslinked Polyimide-based Composite Membranes for Organic Solvent
11 Nanofiltration, *J. Membr. Sci.* 564 (2018) 10-21.

12 [40] B. Su, T. Wang, Z. Wang, X. Gao, C. Gao, Preparation and performance of
13 dynamic layer-by-layer PDADMAC/PSS nanofiltration membrane, *J. Membr. Sci.*
14 423-424 (2012) 324-331.

15 [41] J.S.W. W. Richard Bowen*, Modelling of membrane nanofiltration—pore size
16 distribution effects, *Chem. Eng. Sci.* 57 (2002) 1393–1407.

17 [42] J.S.W. W.R. Bowen, Modelling the performance of membrane nanofiltration—
18 critical assessment and model development, *Chem. Eng. Sci.* 57 (2002) 1121–1137.

19 [43] A.L. Zydney, P. Aimar, M. Meireles, J.M. Pimbley, G. Belfort, Use of the log-
20 normal probability density function to analyze membrane pore size distributions:
21 functional forms and discrepancies, *J. Membr. Sci.* 91 (1994) 293-298.

22 [44] G. Belfort, J.M. Pimbley, A. Greiner, K.Y. Chung, Diagnosis of membrane fouling
23 using a rotating annular filter. 1. Cell culture media, *J. Membr. Sci.* 77 (1993) 1-22.

24 [45] P.C. C.R. Wilke, Correlation of diffusion coefficients in dilute solutions, *AIChE*
25 *J.* 1 (1995) 264-270.

26 [46] A. Cihanoğlu, S. Alsoy Altinkaya, A facile approach for preparation of positively
27 charged nanofiltration membranes by in-situ crosslinking between polyamide-imide
28 and polyethylenimine, *Sep. Purif. Technol.* (2018).

29 [47] I. Soroko, M.P. Lopes, A. Livingston, The effect of membrane formation
30 parameters on performance of polyimide membranes for organic solvent nanofiltration
31 (OSN): Part A. Effect of polymer/solvent/non-solvent system choice, *J. Membr. Sci.*
32 381 (2011) 152-162.

33 [48] C. Tang, Y. Kwon, J. Leckie, Probing the nano- and micro-scales of reverse
34 osmosis membranes—A comprehensive characterization of physiochemical properties
35 of uncoated and coated membranes by XPS, TEM, ATR-FTIR, and streaming potential
36 measurements, *J. Membr. Sci.* 287 (2007) 146-156.

37 [49] J. Gao, S.-P. Sun, W.-P. Zhu, T.-S. Chung, Polyethyleneimine (PEI) cross-linked
38 P84 nanofiltration (NF) hollow fiber membranes for Pb²⁺ removal, *J. Membr. Sci.* 452
39 (2014) 300-310.

40 [50] P. Salehian, M.L. Chua, M. Askari, G.M. Shi, T.-S. Chung, In situ regulation of
41 micro-pore to design high performance polyimide membranes for pervaporation
42 dehydration of isopropanol, *J. Membr. Sci.* 493 (2015) 299-310.

43 [51] L. Xu, J. Xu, B. Shan, X. Wang, C. Gao, Novel thin-film composite membranes
44 via manipulating the synergistic interaction of dopamine and m-phenylenediamine for

1 highly efficient forward osmosis desalination, *J. Mater. Chem. A* 5 (2017) 7920-7932.
2 [52] Y. Hai, J. Zhang, C. Shi, A. Zhou, C. Bian, W. Li, Thin film composite
3 nanofiltration membrane prepared by the interfacial polymerization of 1,2,4,5-benzene
4 tetracarbonyl chloride on the mixed amines cross-linked poly(ether imide) support, *J.*
5 *Membr. Sci.* 520 (2016) 19-28.
6 [53] L. Shen, J. Zuo, Y. Wang, Tris(2-aminoethyl)amine in-situ modified thin-film
7 composite membranes for forward osmosis applications, *J. Membr. Sci.* 537 (2017)
8 186-201.
9 [54] Z. Wang, Z. Wang, S. Lin, H. Jin, S. Gao, Y. Zhu, J. Jin, Nanoparticle-templated
10 nanofiltration membranes for ultrahigh performance desalination, *Nat. Commun.* 9
11 (2018) 2004.
12 [55] S.C. Zhe Tan, Xinsheng Peng, Lin Zhang, Congjie Gao, Polyamide membranes
13 with nanoscale Turing structures for water purification, *Science* 360 (2018) 518–521.
14 [56] A.V. Volkov, V.V. Parashchuk, D.F. Stamatialis, V.S. Khotimsky, V.V. Volkov,
15 M. Wessling, High permeable PTMSP/PAN composite membranes for solvent
16 nanofiltration, *J. Membr. Sci.* 333 (2009) 88-93.
17 [57] L. Zhao, P.C.Y. Chang, C. Yen, W.S.W. Ho, High-flux and fouling-resistant
18 membranes for brackish water desalination, *J. Membr. Sci.* 425-426 (2013) 1-10.
19 [58] Z.J. Santanu Karan, Andrew G. Livingston, Sub-10nm polyamide nanofilms with
20 ultrafast solvent transport for molecular separation, *Science* 348 (2015) 1347-1351.
21 [59] C. Klaysom, S. Hermans, A. Gahlaut, S. Van Craenenbroeck, I.F.J. Vankelecom,
22 Polyamide/Polyacrylonitrile (PA/PAN) thin film composite osmosis membranes: Film
23 optimization, characterization and performance evaluation, *J. Membr. Sci.* 445 (2013)
24 25-33.
25 [60] V. Freger, Kinetics of Film Formation by Interfacial Polycondensation, *Langmuir* :
26 the ACS journal of surfaces and colloids 21 (2005) 1884-1894.
27 [61] J. Xu, H. Yan, Y. Zhang, G. Pan, Y. Liu, The morphology of fully-aromatic
28 polyamide separation layer and its relationship with separation performance of TFC
29 membranes, *J. Membr. Sci.* 541 (2017) 174-188.
30 [62] C. Van Goethem, R. Verbeke, S. Hermans, R. Bernstein, I.F.J. Vankelecom,
31 Controlled positioning of MOFs in interfacially polymerized thin-film nanocomposites,
32 *J. Mater. Chem. A* 4 (2016) 16368-16376.
33 [63] H. Ma, C. Burger, B.S. Hsiao, B. Chu, Highly Permeable Polymer Membranes
34 Containing Directed Channels for Water Purification, *ACS Macro. Lett.* 1 (2012) 723-
35 726.
36 [64] W. Mu, J. Liu, J. Wang, H. Mao, X. Wu, Z. Li, Y. Li, Bioadhesion-inspired
37 fabrication of robust thin-film composite membranes with tunable solvent permeation
38 properties, *RSC Adv.* 6 (2016) 103981-103992.
39 [65] M. Razali, C. Didaskalou, J.F. Kim, M. Babaei, E. Drioli, Y.M. Lee, G. Szekely,
40 Exploring and Exploiting the Effect of Solvent Treatment in Membrane Separations,
41 *ACS applied materials & interfaces* 9 (2017) 11279-11289.
42 [66] P. Gorgojo, M.F. Jimenez-Solomon, A.G. Livingston, Polyamide thin film
43 composite membranes on cross-linked polyimide supports: Improvement of RO
44 performance via activating solvent, *Desalination* 344 (2014) 181-188.

- 1 [67] H. Mariën, I.F.J. Vankelecom, Transformation of cross-linked polyimide UF
- 2 membranes into highly permeable SRNF membranes via solvent annealing, J. Membr.
- 3 Sci. 541 (2017) 205-213.
- 4